

Triple-Function Electrolyte Regulation toward Advanced Aqueous Zn-Ion Batteries

Junnan Hao, Libei Yuan, Yilong Zhu, Mietek Jaroniec, and Shi-Zhang Qiao*

The poor Zn reversibility has been criticized for limiting applications of aqueous Zn-ion batteries (ZIBs); however, its behavior in aqueous media is not fully uncovered yet. Here, this knowledge gap is addressed, indicating that Zn electrodes face a O_2 -involving corrosion, besides H_2 evolution and dendrite growth. Differing from aqueous Li/Na batteries, removing O_2 cannot enhance ZIB performance because of the aggravated competing H_2 evolution. To address Zn issues, a one-off electrolyte strategy is reported by introducing the triple-function $C_3H_7Na_2O_6P$, which can take effects during the shelf time of battery. It regulates H^+ concentration and reduces free-water activity, inhibiting H_2 evolution. A self-healing solid/electrolyte interphase (SEI) can be triggered before battery operation, which suppresses O_2 adsorption corrosion and dendritic deposition. Consequently, a high Zn reversibility of 99.6% is achieved under a high discharge depth of 85%. The pouch full-cell with a lean electrolyte displays a record lifespan with capacity retention of 95.5% after 500 cycles. This study not only looks deeply into Zn behavior in aqueous media but also underscores rules for the design of active metal anodes, including Zn and Li metals, during shelf time toward real applications.

devices benefiting from their advantages in low manufacturing costs and safety performance.^[1] Nevertheless, aqueous batteries still face huge challenges because of their limited energy density ($<40 \text{ Wh kg}^{-1}$) as a result of the narrow working window of 1.23 V.^[2] Thanks to its high overpotential to the water-induced hydrogen (H_2) evolution,^[3] metallic Zn with a high theoretical capacity of 820 mA h g^{-1} can be directly employed as an anode in mild aqueous media.^[4] This can not only theoretically broaden the voltage window of Zn-ion batteries (ZIBs) to 1.79 V, but also significantly simplify the battery manufacturing technology, making ZIBs a promising candidate among aqueous batteries.^[5]

Although the utilization of Zn brings a breakthrough for aqueous batteries, Zn anodes are not perfectly satisfactory even in mild electrolytes due to the widely-reported dendrite growth and H_2 evolution reaction (HER).^[6] These issues

significantly decrease the Coulombic efficiency (CE) of Zn electrodes and shorten the battery lifespan.^[7] To address HER and dendrite growth, the considerable efforts have been made.^[8] From the perspective of Zn electrodes, various solid/electrolyte interphase (SEI) layers have been ex situ/in situ built on Zn surface.^[6,9] These layers suppress the water-induced H_2 evolution by blocking the electrolyte from Zn electrode surface, and facilitate the dendrite-free deposition via providing channels for Zn^{2+} transportation.^[10] Unfortunately, the Zn metal experiences significant volume change upon cycling, which easily causes cracking and shedding of the artificial interphase.^[11] These artificial SEI layers without self-healing ability would gradually lose their functions after long-term cycling.^[12] From the perspective of electrolyte, the first-priority strategy is the use of highly-concentrated electrolyte to reduce the water activity and to regulate the Zn deposition.^[5,13] Nevertheless, highly-concentrated electrolytes sharply increase costs, which discourages their widespread application.^[14] Alternatively, a series of organic electrolyte additives have been proposed.^[15] Despite some improvement in Zn reversibility, these additives likely increases the flammable risk of electrolyte, which compromises the safety advantages of aqueous ZIBs.^[16] Thus, designing low-cost and safe strategy to solve Zn problems is highly desirable for the development of the next-generation ZIBs.

It is worth noting that most of Zn anode studies mainly paid attention to the macroscopic improvements in the reversibility


1. Introduction

As alternatives to Li-ion batteries, aqueous batteries have been regarded as the next-generation large-scale energy storage

J. Hao, Y. Zhu, S.-Z. Qiao
School of Chemical Engineering and Advanced Materials
The University of Adelaide
Adelaide, South Australia 5005, Australia
E-mail: s.qiao@adelaide.edu.au

L. Yuan
Institute for Superconducting and Electronic Materials
Australian Institute for Innovative Materials
University of Wollongong
Wollongong, New South Wales 2522, Australia

M. Jaroniec
Department of Chemistry and Biochemistry and Advanced
Materials and Liquid Crystal Institute
Kent State University
Kent, OH 44242, USA

 The ORCID identification number(s) for the author(s) of this article can be found under <https://doi.org/10.1002/adma.202206963>.

© 2022 The Authors. Advanced Materials published by Wiley-VCH GmbH. This is an open access article under the terms of the Creative Commons Attribution License, which permits use, distribution and reproduction in any medium, provided the original work is properly cited.

DOI: 10.1002/adma.202206963

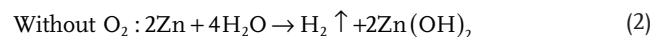
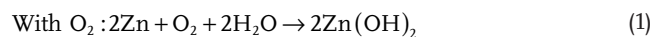
and lifespan of Zn electrode; however, a little attention was paid to revealing the fundamental issues faced by Zn metal.^[7b] To date, challenges still exist in achieving a complete understanding of Zn side reactions in aqueous media. For example, does the metallic Zn electrode experience the oxygen (O₂) adsorption corrosion to consume active Zn? Is it necessary to remove O₂ in the electrolyte before assembling ZIBs? These fundamental issues need to be figured out prior designing high-performance Zn anodes. In addition, another challenge is the spontaneity of the side reactions, leading to the active Zn consumption and by-product accumulation during the shelf time or transportation of battery. Unfortunately, these side reactions would not stop until the active Zn is completely consumed. Thus, inhibiting side reactions of Zn anode during battery rest is of great importance, which has not attracted attention in previous studies.

Here, we studied Zn behavior using a moisture-tolerable glovebox, revealing that the metallic Zn constantly faces O₂ adsorption corrosion, leading to the sustained consumption of Zn electrodes. Unlike traditional aqueous Li/Na batteries, removing O₂ cannot improve the battery performance, since the competitive reaction of HER will be significantly aggravated. To effectively address these issues, a triple-benefit electrolyte additive of sodium glycerophosphate (C₃H₇Na₂O₆P, SG) was proposed. Differing from traditional strategies, this additive can take effect before battery operation by regulating pH value and diminishing free-water activity, which helps to suppress HER and the parasitic by-product accumulation. Meanwhile, metallic Zn could trigger the decomposition of C₃H₇O₆P²⁻ in the inner Helmholtz plane to in situ form a SEI layer on its surface. When the SEI layer fully covered Zn surface, the decomposition of C₃H₇O₆P²⁻ would be stopped until the fresh Zn was exposed, which makes the SEI self-repairable. Accordingly, a side-reaction-free and dendrite-free Zn anode was achieved, resulting in a highly reversible Zn anode with a CE of ≈99.6% under a high depth of discharge (DOD) of 85%. Even with a lean electrolyte, both polyaniline (PANI)/Zn coin and pouch cells feature excellent cycling life (1400 and 500 cycles, respectively).

The pure water and ZnSO₄ solution were selected as typical aqueous media to reveal the common issues faced by all aqueous Zn-based systems. Accordingly, four media were prepared: pure water, pure water without O₂, 2 M ZnSO₄ solution, and 2 M ZnSO₄ without O₂ using a moisture-tolerable and O₂-free glovebox. Subsequently, Zn foils with uniform size were soaked in four electrolytes for one week, which were marked as S-1, S-2, S-3, and S-4, respectively (Figure 1a). As presented in Figure S1, Supporting Information, both S-1 and S-2 electrodes in pure water generate the white by-products, which were collected to perform Raman measurements (Figure 1b). Results show two strong bands at 367 and 381 cm⁻¹ attributed to the symmetric Zn–O stretching of the ZnO₄ tetrahedron,^[17] and one weak band at 479 cm⁻¹ assigned to the translational mode of –OH vibration, manifesting the by-product of Zn(OH)₂.^[18]

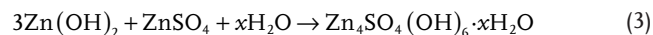
It is worth noting that gas bubbles were generated on Zn electrodes during the shelf time no matter whether in pure water or ZnSO₄ electrolyte (Figure S2, Supporting Information), indicating the occurrence of HER evidenced by gas chromatography (GC) analysis (Figure 1c). Interestingly, the H₂ amount was significantly higher in both water and ZnSO₄ systems after

removing O₂ (from 15 299 to 58 421 ppm in water, and from 63 606 to 177 513 ppm in ZnSO₄, Figure 1d). These results show that O₂ in aqueous electrolytes affects the Zn behavior and HER. The side reactions of Zn electrodes in aqueous media with/without O₂ can be expressed as follows,



The O₂-involving side reaction can be defined as O₂ adsorption corrosion of Zn electrodes, which consumes the active Zn. When the electrolyte contains O₂, Zn electrodes will undergo O₂ adsorption corrosion (Equation (1)). Once the O₂ in electrolyte is consumed, the Zn electrode will directly react with water to generate H₂ (Equation (2)). Thus, the O₂ adsorption corrosion of Zn electrode can also be regarded as a competitive reaction of HER.

To identify the by-product species generated in the ZnSO₄ electrolyte, Raman spectra were collected (see Figure 1e). Differing from Zn(OH)₂ by-product in water, another by-product of Zn₄SO₄(OH)₆·xH₂O was formed in ZnSO₄ electrolyte,^[19] as confirmed by Raman and XRD results (Figures 1e,f). This also confirms that Zn(OH)₂ is unstable in the ZnSO₄ electrolyte, and transform into Zn₄SO₄(OH)₆·xH₂O (Equation (3)).^[20]



The by-product accumulation of Zn(OH)₂ in pure water and Zn₄SO₄(OH)₆·xH₂O in the ZnSO₄ electrolyte are further evidenced by Fourier transform infrared (FTIR) measurements, revealing the thermodynamic instability of Zn electrodes in all water-based electrolytes (Figure S3, Supporting Information). As summarized in Figure 1g, O₂ adsorption corrosion, HER, and their parasitic by-product accumulation significantly affect the Zn stability in aqueous electrolytes during battery rest.

The Zn surface evolution caused by O₂ effects were studied by laser confocal scanning microscopy and scanning electron microscope (SEM). In pure water with O₂, the 3D confocal image of the S-1 electrode shows abundant needlelike by-products (Figure 1h). After the removal of O₂, less visible by-products are generated on the surface of S-2 (Figure 1i), indicating that the existence of O₂ in water boosts the accumulations of Zn(OH)₂. Interestingly, the tendency is different in ZnSO₄ electrolyte (Figure 1j,k), which is confirmed by SEM images (Figure 1l–o). In this case, the accumulation of Zn(OH)₂ fine particles on Zn electrodes is loose. They are easily peeled off from Zn substrates due to the poor adhesion, as evidenced by optical image after two-month soaking (Figure S4, Supporting Information). Thus, Zn(OH)₂ by-products cannot stop the corrosion reactions of Zn electrodes in pure water, which is similar to loose Zn₄SO₄(OH)₆·xH₂O by-product sheets (Figure S5, Supporting Information). Thus, without protection, the O₂ adsorption corrosion and HER continuously consume Zn until it is fully reacted.

In addition to the state of battery rest, O₂ effects on Zn behavior were also studied during battery operation because the necessity of eliminating O₂ in aqueous ZIBs is always controversial.^[8a] Figure 2a shows Zn stripping/plating curves

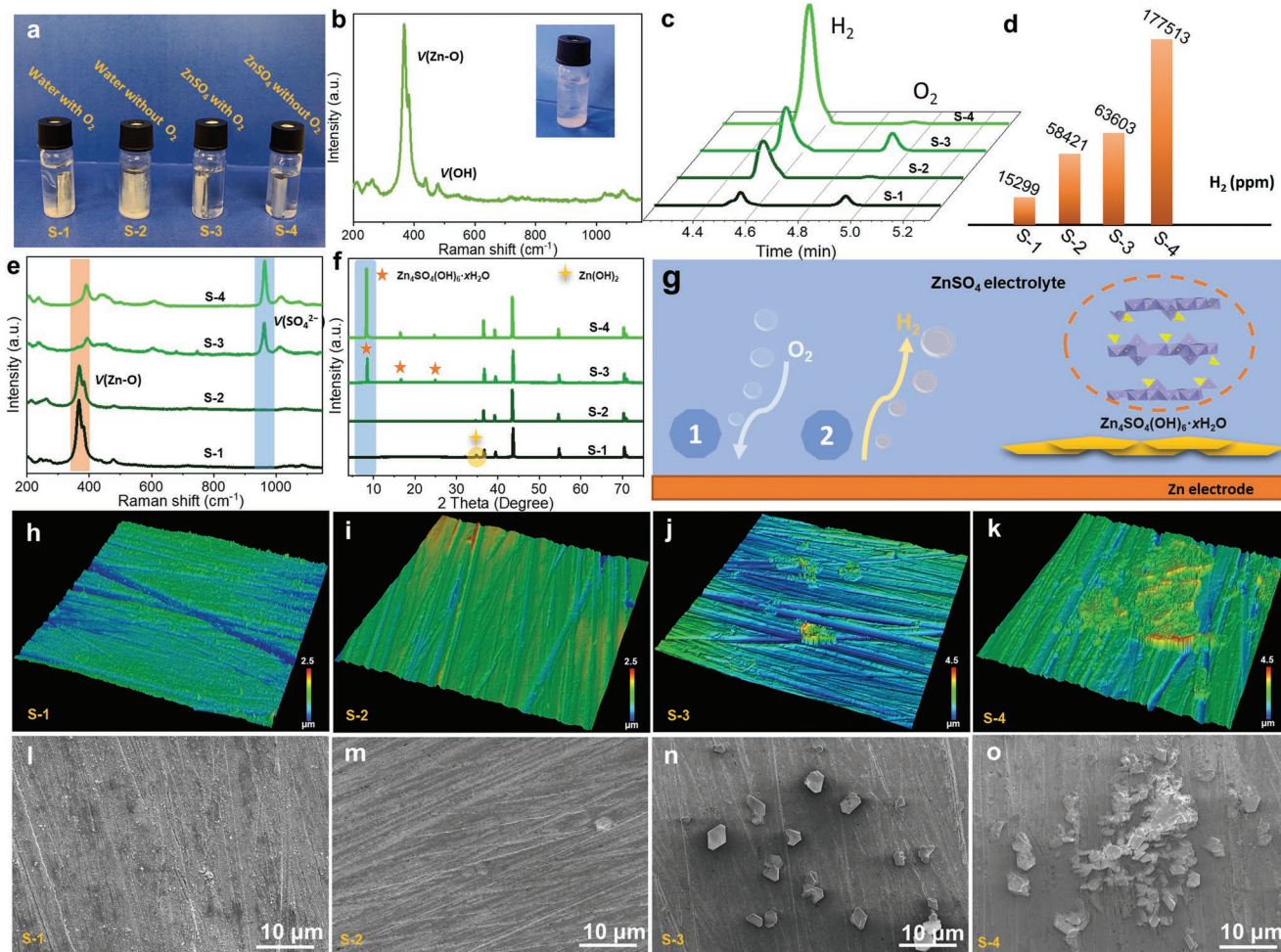


Figure 1. Fundamental study on Zn behavior during the shelf time. a) Zn foils soaked in different aqueous media. b) Raman spectrum of the by-product generated in pure water. c) GC curves to test the H₂ evolution in different aqueous media after one week soaking. d) The specific H₂ amount generated in four media. e) Raman spectra of Zn foils after soaking in different media. f) XRD patterns of Zn foils soaked in various media. g) Schematic diagram illustrating issues faced by the Zn electrode to affect its stability during battery rest. h–k) 3D confocal images for Zn electrodes after one-week soaking in pure water (h), pure water without O₂ (i), 2 M ZnSO₄ (j), and 2 M ZnSO₄ without O₂ (k). l–o) SEM images for Zn electrodes after one-week soaking in pure water (l), pure water without O₂ (m), 2 M ZnSO₄ (n), and 2 M ZnSO₄ without O₂ (o).

in 2 M ZnSO₄ with O₂ under 2.5 mA cm⁻² and according in situ GC curves. Results reveal a stable polarization value of Zn plating/stripping with the increased H₂ evolution upon cycling (see Figure 2a). The intensity of H₂ evolution increases from 18.6 to 40.1 ppm after 3.5 cycles (Figure S6, Supporting Information). After removing O₂ in ZnSO₄ electrolyte (Figure S7, Supporting Information), the cell shows a fluctuated voltage polarization of Zn plating/stripping with the aggravated H₂ evolution from 22.5 ppm at the beginning to 50.2 ppm after 3.5 cycles (Figure 2b). Hence, removing O₂ exacerbates HER in ZIBs and further affects the performance of aqueous ZIB system. This finding reveals that O₂ effects on aqueous ZIBs are different from the traditional aqueous Li/Na batteries.^[1a] Figure 2c shows the rotating disk electrode (RDE) measurements for Zn electrodes in ZnSO₄ electrolyte with/without O₂ under a rotation rate of 1600 rpm. No current polarization can be recorded for the Zn electrode in ZnSO₄ without O₂ in the whole potential window from 0.2 to -0.6 V versus saturated

calomel electrode (SCE), however, there is an obvious current polarization at -0.2 V versus SCE, which corresponds to the O₂ reduction. This elucidates that O₂ involves side reactions of Zn electrodes during battery operation.

Currently, aqueous ZIBs are generally assembled in air, which helps to reduce the manufacturing costs. To truthfully reflect overall effects of O₂ adsorption, HER, and dendrite growth on Zn electrodes, the Cu/Zn cells assembled in air were tested under different DODs (with a commonly preferred 100 μm). With a super low DOD of 0.85% (1 mA cm⁻² and 0.5 mA h cm⁻²), the cell shows a conspicuous CE fluctuation after ≈170 cycles at 30 °C, indicating a battery failure (Figure 2d).^[21] Moreover, the Zn plating/stripping shows a low initial CE of 67.4% and average CE of 96.9%, indicating its low reversibility induced by the O₂ corrosion, HER, and dendrite formation. After removing the O₂, however, the CE and cycling life of Zn electrodes in 2 M ZnSO₄ electrolyte were reduced to 94.6% and 110 cycles, respectively (Figure S8, Supporting

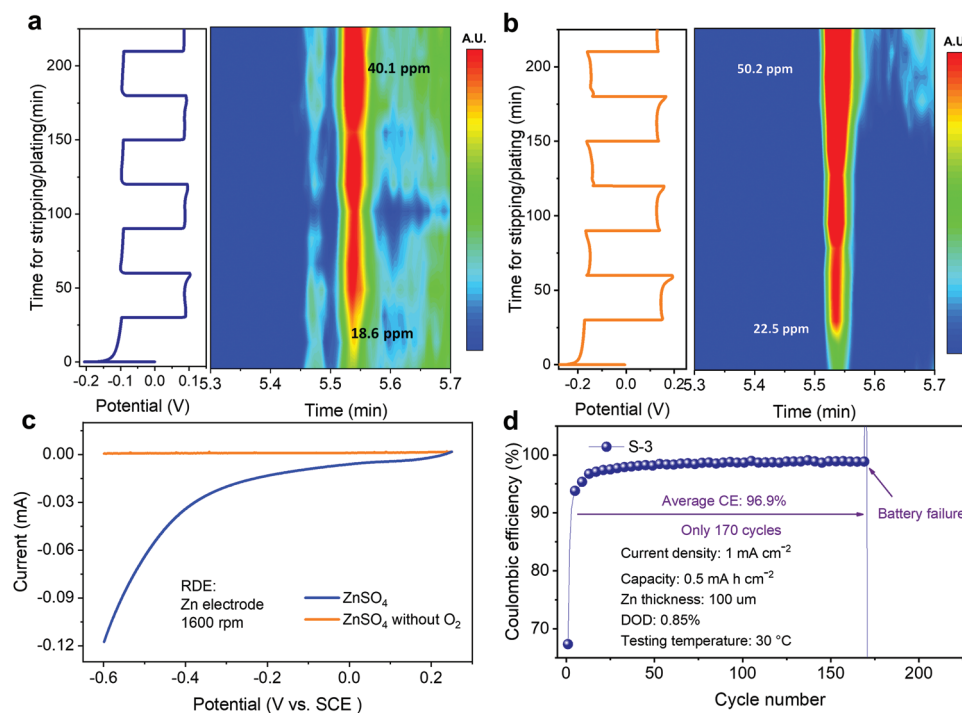


Figure 2. Zn reversibility studies during battery operation. a,b) Zn stripping/plating curves and according in situ GC curves to evaluate H₂ evolution within the electrolyte of 2 M ZnSO₄ with O₂ (a) and without O₂ (b). c) RDE measurements of Zn electrode in ZnSO₄ electrolyte with/without O₂ under a rotation rate of 1600 rpm. d) The Zn reversibility in Cu/Zn cells assembled in air under a DOD of 0.85%.

Information). Such limited lifespan and reversibility of Zn electrodes with low Zn utilizations are far from satisfactory to meet the demands of aqueous ZIBs for practical applications.

For an ideal situation, side reactions of Zn anodes should be prevented before battery operation. Otherwise, they will unremittingly consume the active Zn anode and damage the cell during battery rest or transportation. Unfortunately, previous electrolyte strategies have not paid much attention on addressing Zn issues before battery operation.^[8b,12b] Here, we propose a triple-function electrolyte additive of SG to solve Zn battery issues during the shelf time. To understand how the SG additive works on Zn electrodes during battery rest, the pH values of ZnSO₄ electrolyte, pure SG solution, and hybrids were measured (Figure 3a). These measurements show that 2 M ZnSO₄ electrolyte is slightly acidic with a pH value of 4.72. For the pure 0.5 M SG solution, a higher pH value of 8.30 is achieved, therefore SG can function as a pH regulator. For the ZnSO₄ electrolyte with 0.01 M SG, the pH value increases to 5.13, indicating the H⁺ concentration is reduced. The pH value of the electrolyte solution raises to 5.18, 5.20, and 5.23 along with increasing SG concentration to 0.05, 0.1, and 0.5 M, respectively, which dynamically benefits the suppression of H₂ evolution corrosion. Moreover, SG features abundant oxygen-containing functional groups based on its unique structure (Figure S9, Supporting Information), which can form the H-bond with water molecules in the ZnSO₄ electrolyte to reduce the water activity and further suppress HER.

A series of Zn electrodes were soaked in 2 mL of 2 M ZnSO₄ with/without 0.05 M SG to compare the Zn surface evolution along with soaking time from 2 days to 20 days (Figure S10, Supporting Information). In the pure ZnSO₄ electrolyte, the

Zn surface gradually changes from the bright metallic color into dark gray, revealing the progressively aggravated corrosion reactions (Figure 3b upper). However, Zn metal surface maintains a light gray color with 0.05 M additive. To determine the species generated on Zn electrodes, the ex situ XRD patterns were conducted. As can be seen from Figure 3c, the pattern of Zn electrode soaked in pure ZnSO₄ electrolyte for 2 days shows the main Zn peaks at 36.3°, 39.0°, 43.2°, and 54.3°. After soaking for 6 days, the peak of Zn₄SO₄(OH)₆·xH₂O by-product at 8.9° is remarkable (Figure S11a, Supporting Information), and its intensity increases sharply along with prolonged soaking time.^[22] After 20 days, the (002) peak intensity of Zn₄SO₄(OH)₆·xH₂O is much higher than those of Zn metal, indicating that side reactions ruin the Zn electrode. In comparison, patterns of Zn soaked in the SG-containing electrolyte mainly show Zn peaks without obvious by-product formation (Figure 3d). The zoom-in pattern in Figure S11b, Supporting Information shows a peak at 6.5° with a low intensity after 10 days soaking, corresponding to the (002) face of Zn₃(PO₄)₂-based product. This indicates the spontaneous formation of SEI on the Zn surface during the shelf time, which was also confirmed by FTIR spectra (Figure 3e).^[23] Importantly, after prolonging the soaking time to 20 days, there is no visible intensity changes in the SEI peak on ex situ XRD patterns (Figure S11b, Supporting Information), indicating its stable thickness.

The thickness is one of vital parameters for SEI layers; however, challenges still exist in building a thin SEI layer allowing fast Zn²⁺ transfer.^[8a] To assess the thickness of our SEI layer, the focused ion beam (FIB) was conducted on the soaked Zn electrode (20 days) to obtain the smooth cross-section (Figure 3f). A Pt layer was introduced to protect the artificial

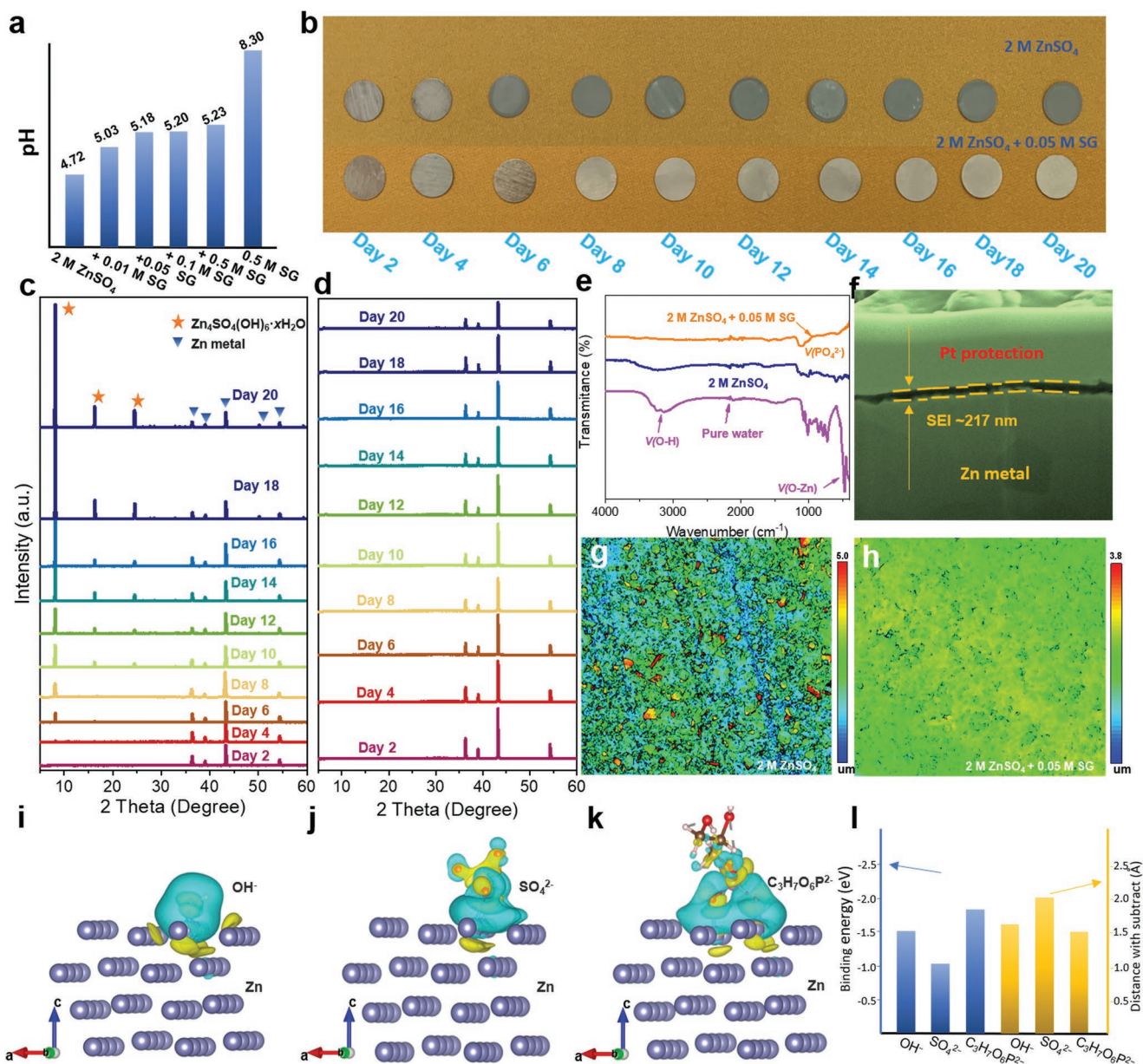


Figure 3. Sodium glycerophosphate (SG) additive effects on side reactions of the Zn anode under battery rest. a) pH values of ZnSO₄ electrolyte and ZnSO₄ electrolyte with various contents of additive. b) Digital image of Zn foils immersed in 2 M ZnSO₄ with/without 0.05 M SG. c,d) Ex situ XRD patterns of soaked Zn foils to study the by-product formation in 2 M ZnSO₄ (c) and 2 M ZnSO₄ + 0.05 M SG (d). e) FTIR spectra of Zn foils soaked in pure water and 2 M ZnSO₄ with/without 0.05 M SG. f) Cross-section view of Zn foils soaked in the electrolyte for 20 days after FIB cutting, showing the thickness of ≈217 nm of SEI layer. g,h) 2D confocal images of Zn foils immersed in 2 M ZnSO₄ (g) and 2 M ZnSO₄ + 0.05 M SG (h). i–k) Optimized geometry and the corresponding differential charge density distributions of Zn substrate–OH⁻ (i), Zn substrate–SO₄²⁻ (j), and Zn substrate–C₃H₇O₆P₂⁻ (k). The unit of isosurface values is shown in this figure. Carbon, nitrogen, copper, and oxygen atoms are green, blue, gold, and red, correspondingly. Yellow represents electron accumulation and cyan denotes electron depletion. l) Binding energy as well as the distance of OH⁻, SO₄²⁻, and C₃H₇O₆P₂⁻ from the Zn substrate.

layer since the high-energy beamline could possibly damage it.^[24] Energy-dispersive spectroscopy (EDS) results in Figure S12, Supporting Information show that the SEI layer contains elements of Zn, O, and P. The thickness of SEI is ≈217 nm, much thinner than the reported SEI layers on Zn electrodes.^[8d,25] 2D confocal images of Zn electrodes after soaking for 20 days in ZnSO₄ electrolyte with/without 0.05 M SG were compared. In pure ZnSO₄ electrolyte, massive by-product plates

are generated on the Zn surface due to serious side reactions (Figure 3g). However, the Zn surface is clean and homogenous in the SG-containing electrolyte, indicating that side reactions are effectively inhibited (Figure 3h). Moreover, Zn/Zn pouch cells were compared to assess the effectiveness of SG additive during the shelf time (Figure S13, Supporting Information). For the pure ZnSO₄ electrolyte, the pouch cell shows an obvious swelling after resting for two months. In contrast, the

Zn/Zn pouch cell with the SG additive-containing electrolyte does not show obvious change, indicating that side reactions can be effectively suppressed under the state of battery rest, which paves the way toward practical applications of ZIBs.

To understand the mechanism of SEI formation on Zn electrodes in the electrolyte of ZnSO₄ with SG, the density functional theory (DFT) calculations were conducted to reveal the ion distribution in the inner Helmholtz plane of Zn electrodes. The components of the inner Helmholtz plane are strongly related to the SEI layer formation on the electrode surface.^[26] Figure S14, Supporting Information presents models of Zn slabs with different anions in the electrolyte, including OH⁻, SO₄²⁻, and C₃H₇O₆P²⁻, in which OH⁻ is closely related to O₂ adsorption corrosion of Zn electrodes. Figure 3i–k summarizes geometrical structures with differential charge density distributions and binding energies of these interactions. The large binding energies of anions are induced by the as-formed strong Zn–O/P/S interactions as well as a significant charge transfer. Compared to OH⁻ (–1.48 eV) and SO₄²⁻ (–1.02 eV), C₃H₇O₆P²⁻ has larger binding energy with the Zn slab (–1.64 eV, Figure 3l left). In addition, the O atom in C₃H₇O₆P²⁻ anion also features a shorter distance of 1.49 Å with the Zn substrate than that with OH⁻ (1.53 Å) and SO₄²⁻ (1.99 Å), indicating that C₃H₇O₆P²⁻ ions mainly dominate in the inner Helmholtz plane of the Zn electrode (Figure 3l right). Notably, the charge density of C₃H₇O₆P²⁻ anion significantly shifts after immobilization on the Zn slab, as evidenced by images of differential charge density (Figure S15a,b, Supporting Information). The re-distribution of charge density triggers the hydrolysis of the adsorbed C₃H₇O₆P²⁻ into PO₄²⁻ and glycerin (C₃H₆O₃) (Figure S15c, Supporting Information). C₃H₆O₃ can reduce the water activity in the Helmholtz plane to inhibit the H₂ evolution through the formation of H-bond.^[27] Simultaneously, PO₄²⁻-based SEI can be formed on the Zn surface, which blocks OH⁻ and water from the Zn surface to stop the O₂ corrosion and HER. Once the Zn surface is fully covered by the SEI layer, the hydrolysis of C₃H₇O₆P²⁻ would be terminated until the fresh Zn is exposed. As a result, this SEI is heal-repairable with the preserved thickness, as evidenced by previous ex situ XRD results. Once this solid SEI layer cracks or damages, the electrolyte would contact the fresh Zn to repair the SEI layer, which enables its self-healing capability.

The reversibility of Zn stripping/plating in ZnSO₄ electrolytes with different SG concentrations is compared in Cu/Zn cells (Figure S16, Supporting Information and Figure 4a). Under a low DOD of 0.85% (1 mA cm⁻² and 0.5 mA h cm⁻²), the Cu/Zn cell with 0.01 M SG delivers a high initial CE of 86.4%, however, it experiences dramatic fluctuations after 490 cycles caused by the short circuit.^[28] When the concentration of additive increases to 0.05 M, the Cu/Zn cell displays a super long cycling life of 1000 cycles and a high average CE of 99.1%. This performance is overwhelming compared to that of cell with pure ZnSO₄ electrolyte (170 cycles with CE of 96.9%). When the additive concentration increases to 0.1, 0.5, and 1.0 M, however, initial CE values and cycling life for Zn plating/stripping are gradually reduced with higher polarization of Zn plating/stripping (Figure S17, Supporting Information). The optimal concentration also prolongs the lifespan of Zn/Zn cell from ≈200 h to over 1000 h under 1 mA cm⁻² and 1 mA h cm⁻² (Figure S18, Supporting Information). To prove

the feasibility of functional electrolyte under strictly practical conditions, a super high DOD of 85% was applied by using a thin Zn electrode (10 μm) (Figure 4b). Under this high DOD, the Cu/Zn cell shows the CE fluctuations after only 30 cycles in 2 M ZnSO₄, which demonstrates the limited Zn lifespan due to the rapid Zn consumption. During 30 cycles, the average CE is only 98.3%. In comparison, the Cu/Zn cell with 10 μm Zn foil shows a prolonged cycling life for over 100 cycles with a high CE of 99.6% in the SG-containing electrolyte, which demonstrates the effectiveness of SG under a strict working standard.

To verify the practicability of SG additive under battery operation, multiple measurements were conducted. Figure S19, Supporting Information shows RDE measurements of Zn electrode in ZnSO₄ electrolyte with/without SG additive. As mentioned previously, the Zn electrode experiences an obvious O₂ adsorption reaction in pure ZnSO₄ electrolyte. Whereas the current polarization at –0.2 V versus SCE is significantly reduced in 2 M ZnSO₄ + 0.05 M SG, indicating that O₂ adsorption reaction is effectively suppressed.^[29] Figure 4c presents in situ GC results in Zn/Zn cell with the SG-containing electrolyte upon Zn plating/stripping. There is no obvious H₂ signal during the whole 3.5 cycles, which suggests that HER is suppressed during battery operation as well (Figure S20, Supporting Information). The suppressed HER is mainly caused by decreasing H⁺ concentration, the water-activity reduction, and self-healing SEI layer formation induced by SG additive. Figure 4d,e shows in situ pH measurements of the electrolyte during battery operation. In the pure ZnSO₄, the pH value near the counter electrode sharply increases once the Zn plating occurs, indicating the synchronization of HER. The pH value of electrolyte is immediately reduced as the stripping of Zn proceeds, then it gradually increases during the stripping process, which manifests the fluctuation of OH⁻ caused by HER during the whole plating/stripping.^[30] When the electrolyte contains SG additive, the pH value is almost the same due to the non-fluctuation of H⁺ concentration, which further evidences the inhibition of HER.

The morphology of Zn electrodes after 50 cycles in Cu/Zn cells is compared in Figure 4f,g. In the pure ZnSO₄ electrolyte, the excessive by-product sheets are generated on the Zn surface, which not only consumes the active Zn but also shortens the battery lifespan (Figure S21, Supporting Information). In the SG-containing electrolyte, however, side reactions are effectively suppressed. Moreover, the suppressed accumulation of Zn₄SO₄(OH)₆·xH₂O by-product on the cycled Zn electrode is further confirmed by the 3D confocal images (Figure S22, Supporting Information) and XRD patterns (Figure S23, Supporting Information). To identify the chemical environment on the surface of cycled Zn in different electrolytes, X-ray photoelectron spectroscopy (XPS) analysis with depth profiling was performed. No obvious peak shift occurs after depth profiling in Zn 2p curves of Zn electrodes cycled in ZnSO₄ electrolyte (Figure S24, Supporting Information). Whereas the Zn LMM spectra change obviously with new peaks appearance at ≈992.6 and ≈996 eV along with etching, which are indexed to the metallic Zn⁰. However, the Zn²⁺ (≈986.8 eV) peak ascribed to Zn₄SO₄(OH)₆·xH₂O remains during the whole etching process, inducing the massive by-product accumulation (Figure 4h).^[31] The S 2p scan is presented in Figure 4i, showing

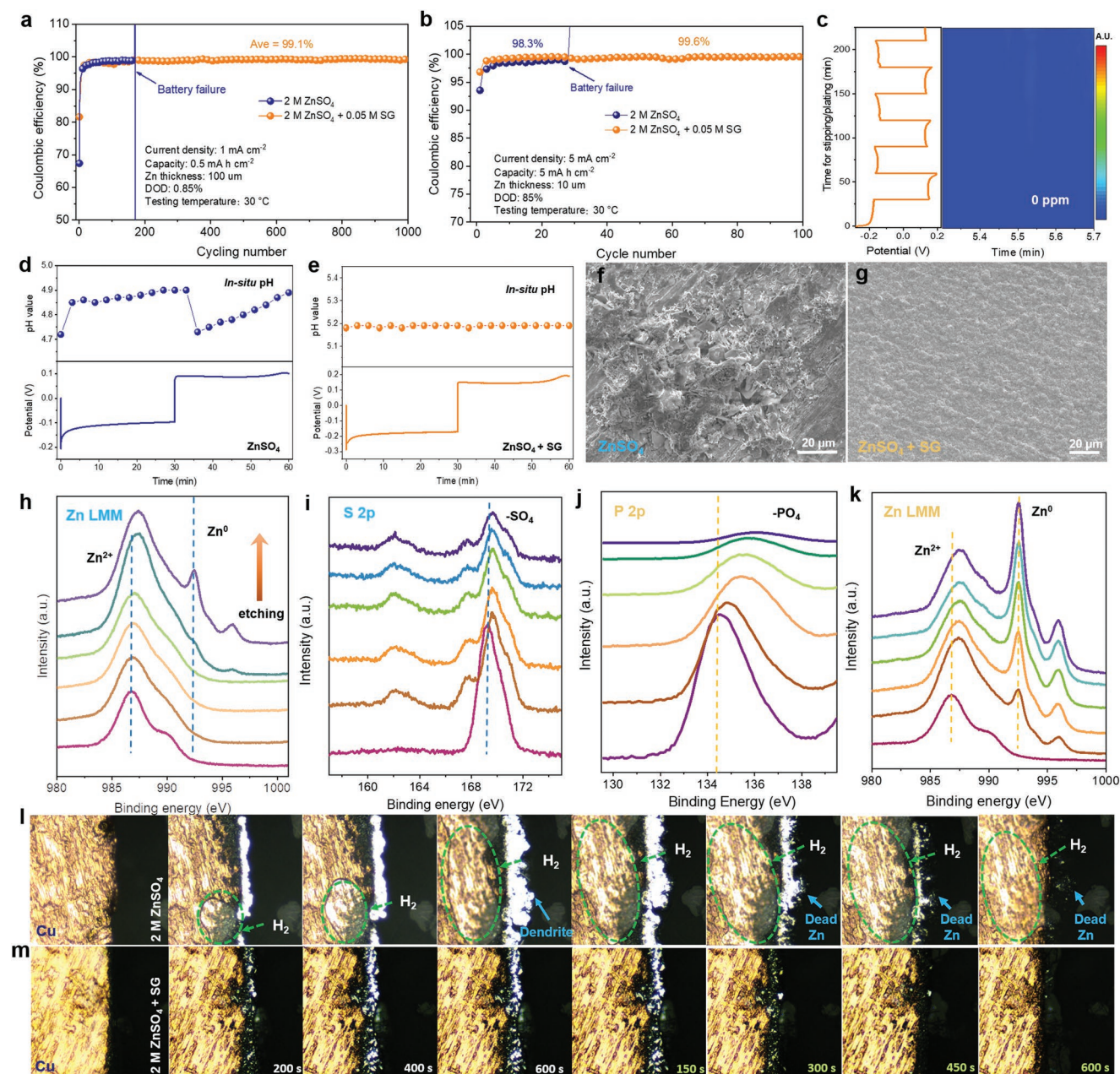


Figure 4. SG additive effects on the Zn reversibility under battery operation. a, b) The Zn reversibility in Cu/Zn cells with/without SG additive under a low DOD of 0.85% (a) and a high DOD of 85% (b). c) In situ GC results to evaluate the H₂ evolution during the Zn/Zn cell cycling in 2 M ZnSO₄ + 0.05 M SG. d, e) In situ pH tests on the court electrode in Zn/Zn cells within 2 M ZnSO₄ (d) and 2 M ZnSO₄ + 0.05 M SG (e). f, g) SEM images of Zn foils after 50 cycles in 2 M ZnSO₄ (f) and 2 M ZnSO₄ + 0.05 M SG (g). h, i) XPS profiles of cycled Zn foils in 2 M ZnSO₄ after different etching depth: h) Zn LMM and i) S 2p. j, k) XPS profiles of cycled Zn foils in 2 M ZnSO₄ + 0.05 M SG after different etching depth: j) P 2p and k) Zn LMM. l, m) In situ optical microscope images of Cu electrode for Zn plating/stripping within 2 M ZnSO₄ (l) and 2 M ZnSO₄ + 0.05 M SG (m).

that the strong SO₄²⁻ peak (≈ 169.3 eV) is gradually reduced with increasing etching depth. Nevertheless, the peak of by-product is still visible even after 250 s etching. In contrast, the P 2p (≈ 134.4 eV) instead of S 2p signal is detected on the surface of Zn cycled in the electrolyte with SG additive (Figure 4j), indicating Zn₄SO₄(OH)₆ · xH₂O by-product is effectively suppressed. The P 2p signal gradually decreases along with etching, which matches well with the evolution of the Zn LMM (Figure 4k), indicating the formation of thin SEI layer.

Specially designed Cu/Zn cells were tested to in situ monitor the morphology of deposited Zn in ZnSO₄ electrolytes with/without SG additive (Figure S25, Supporting Information). In pure ZnSO₄ electrolyte, uneven Zn dendrites along with the serious H₂ evolution appear upon Zn plating, as presented in Video S1, Supporting Information. These dendrites and bubbles remain in the following stripping process, leading to the low Zn reversibility. Typical snapshots taken during the plating/stripping are shown in Figure 4l. The heterogeneous Zn

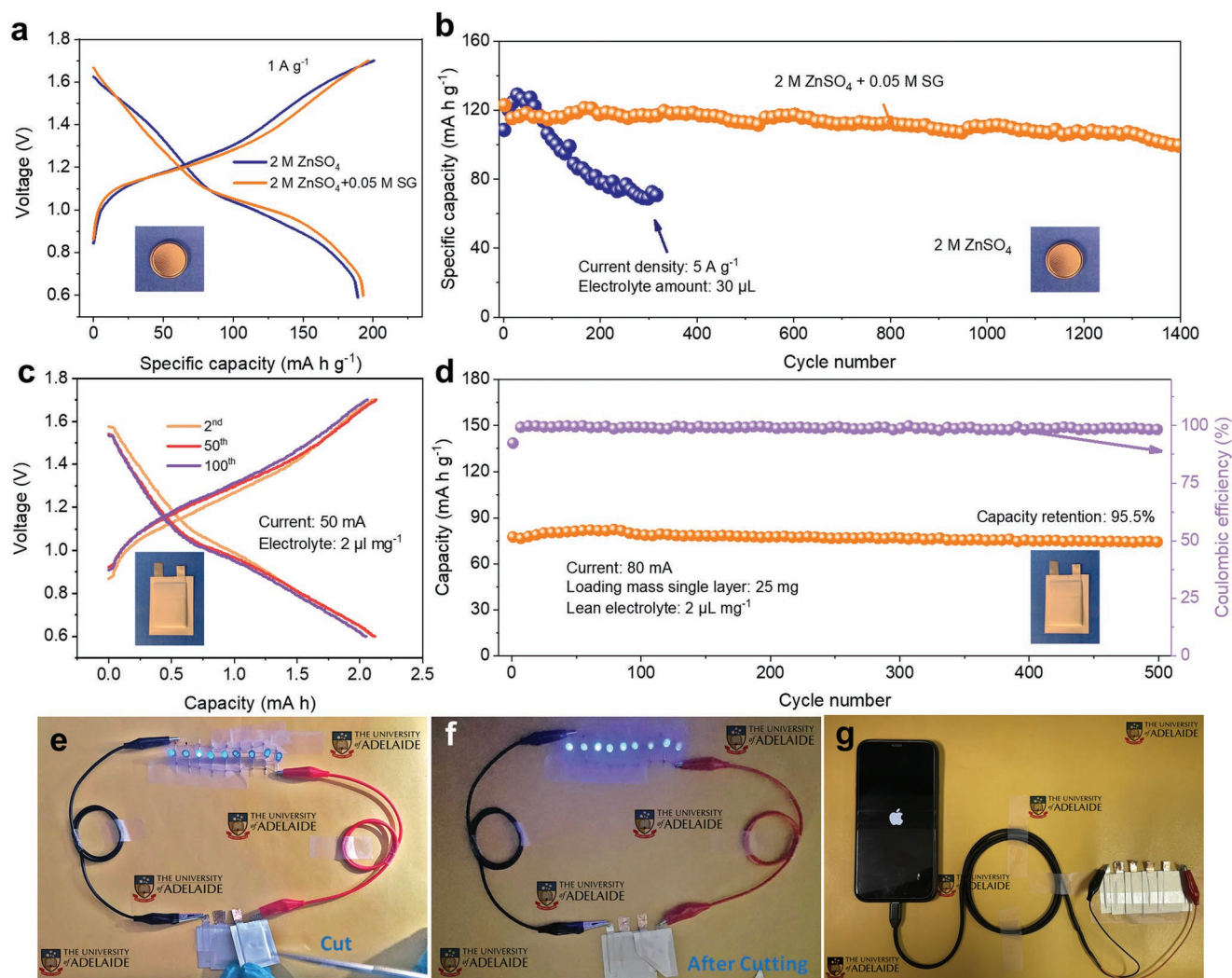


Figure 5. Full-cell characterization. a) Charge–discharge curves for PANI/Zn coin-cells with 2 M ZnSO_4 and $2 \text{ M ZnSO}_4 + 0.05 \text{ M SG}$ under a low current density of 1 A g^{-1} . b) Cycling stability of PANI/Zn coin cells at a high current density of 5 A g^{-1} with different electrolytes, the electrolyte addition is $30 \mu\text{L}$. c) Charge–discharge curves for PANI/Zn pouch-cells with a lean electrolyte addition of $2 \mu\text{L mg}^{-1}$ under a current of 50 mA . d) Cycling stability of PANI/Zn pouch cells at a high current of 80 mA with a lean electrolyte addition of $2 \mu\text{L mg}^{-1}$. e–g) The practicality evaluation of the PANI/Zn pouch cells: e) by illuminating nine blue LEDs, f) by illuminating nine blue LEDs after cutting one cell, indicating the safety performance, and g) by powering an iPhone.

deposition is visible with a bubble after 200 s plating, indicating the dendrite formation and HER. Some protrusions gradually turn into Zn dendrites with further plating (600 s). Upon stripping, the deposited Zn is gradually removed from the Cu electrode, however, obvious HER and residual Zn remain on the Cu electrode even after 600 s stripping. In comparison, the Zn plating on the Cu electrode is smooth and homogeneous in the SG-based ZnSO_4 electrolyte, as illustrated in Video S2, Supporting Information. No obvious Zn dendrites and H_2 evolution are generated after 600 s plating (Figure 4m). After 600 s stripping, the deposited Zn is completely removed from the Cu electrode, which affirms the high reversibility of side-reaction-free and dendrite-free Zn plating/stripping.

PANI/Zn batteries were assembled to assess the function of SG additive on the full-cell performance, where the PANI cathode was in situ grown on the carbon cloth. After the

polymerization reaction, these carbon fibers are fully covered by abundant arrays, indicating the formation of PANI (Figure S26, Supporting Information). The galvanostatic discharge-charge curves of the PANI/Zn coin cell were performed under 1 A g^{-1} , as presented in Figure 5a. In the pure ZnSO_4 electrolyte, the cell displays two discharging plateaux, which indicates the $\text{H}^+/\text{Zn}^{2+}$ co-working mechanism of PANI cathode. In contrast, the second plateau is distinct when the electrolyte contains 0.05 M SG additive, demonstrating the storage of a large amount of Zn^{2+} . Thus, the discharge capacity is slightly enhanced from ≈ 188.2 to $\approx 192.3 \text{ mA h g}^{-1}$. Then the cycling performance in coin cells was tested by controlling the electrolyte addition and compared under a high current density of 5 A g^{-1} , in which $30 \mu\text{L}$ electrolyte was added to just infiltrate separator (Figure 5b). In the pure ZnSO_4 electrolyte, the PANI/Zn coin cell shows a rapid capacity fading after 300 cycles with

the capacity retention of 62.5%. However, the good cycling stability in the electrolyte containing 0.05 M SG is pronounced. After 1400 cycles, a high capacity of 99.5 mA h g⁻¹ remains, corresponding to the retention of ≈81.7%.

It has been widely accepted that the performance evolution under the lean electrolyte is one of the most important steps to fulfil the goal of battery commercialization.^[32] Instead of coin cells, the PANI/Zn pouch cells with 0.05 M SG additive were assembled under the strict environment of the lean electrolyte addition (2 μL mg⁻¹) (Figure S27, Supporting Information). Under the current of 50 mA, the pouch cell with 0.05 M SG additive displays similar charge–discharge curves to these in coin cell, indicating the uniformity of electrochemical performance when the battery was scaled up (Figure 5c). The cycling stability of the pouch cell measured under a high current density of 80 mA is shown in Figure 5d. It can be found that this pouch cell shows a high reversibility of ≈100% CE. After 500 cycles, the capacity remains 95.5%, which is also superior to that reported for PANI/Zn pouch cells.^[33] The efficacy of the pouch cell is demonstrated by using it to power different devices. Three small pouch cells in series can illuminate nine blue light-emitting diodes (LEDs, 3.0 V), as shown in Figure 5e. Importantly, these cells can still power the LEDs after cutting one corner of the cell (Figure 5f), indicating its advantages of high safety performance. Pouch cells in series can also power other devices, such as a rotating fan (Figure S28, Supporting Information) and charging an iPhone (Figure 5g), which demonstrates the high potential of ZIBs with SG additive in practical applications.

In summary, Zn behavior was thoroughly studied in aqueous media, indicating that Zn anodes also face Zn-consuming O₂ adsorption corrosion beside HER and dendrite growth. Differing from traditional aqueous Li/Na batteries, however, removing O₂ cannot enhance the battery performance. The functional additive of SG was introduced in the electrolyte to solve Zn problems. It regulated the H⁺ concentration and diminished free-water activity, significantly inhibiting the H₂ evolution. The hydrolysis of C₃H₇O₆P²⁻ distributed in the inner Helmholtz layer of Zn electrode also triggers the formation of self-repairing SEI with a thickness of ≈217 nm before battery operation, which inhibits O₂ corrosion and dendrite growth. Thus, the high Zn reversibility was achieved even under a high DOD of 85%, which also guarantees the excellent performance of ZIBs in both coin cells and pouch cells. Under the lean electrolyte, the PANI/Zn batteries displayed excellent cycling performance for 1400 and 500 cycles in coin cell and pouch cell, respectively. This work reveals Zn behavior in water-based electrolytes and guides future research to achieve the highly efficient utilization of active metal anodes for future commercialization.

2. Experimental Section

Experimental details can be found in the Supporting Information.

Supporting Information

Supporting Information is available from the Wiley Online Library or from the author.

Acknowledgements

J.H., and L.Y. contributed equally to this work. The authors thank Dr. Chao Ye, Dr. Fangxi Xie, Huan Li, Xin Xu, and Chun-chuan Kao for the helpful discussion. Financial support from the Australian Research Council (ARC) (FL170100154, DP220102596) is gratefully acknowledged. DFT computations were undertaken with the assistance of resources and services from the National Computational Infrastructure (NCI) and Phoenix High Performance Computing, which are supported by the Australian Government and the University of Adelaide.

Open access publishing facilitated by The University of Adelaide, as part of the Wiley - The University of Adelaide agreement via the Council of Australian University Librarians.

Conflict of Interest

The authors declare no conflict of interest.

Data Availability Statement

The data that support the findings of this study are available from the corresponding author upon reasonable request.

Keywords

aqueous batteries, electrolyte modification, O₂ adsorption corrosion, self-healing ability

Received: August 1, 2022

Revised: August 28, 2022

Published online: October 3, 2022

- [1] a) Y. Yamada, J. Wang, S. Ko, E. Watanabe, A. Yamada, *Nat. Energy* **2019**, *4*, 269; b) X. Dong, L. Chen, J. Liu, S. Haller, Y. Wang, Y. Xia, *Sci. Adv.* **2016**, *2*, e1501038; c) J. Hao, L. Yuan, B. Johannessen, Y. Zhu, Y. Jiao, C. Ye, F. Xie, S. Z. Qiao, *Angew. Chem.* **2021**, *133*, 25318.
- [2] J. Xie, Z. Liang, Y.-C. Lu, *Nat. Mater.* **2020**, *19*, 1006.
- [3] a) D. Chao, W. Zhou, F. Xie, C. Ye, H. Li, M. Jaroniec, S.-Z. Qiao, *Sci. Adv.* **2020**, *6*, eaba4098; b) D. Kundu, B. D. Adams, V. Duffort, S. H. Vajargah, L. F. Nazar, *Nat. Energy* **2016**, *1*, 16119.
- [4] a) Q. Zhao, W. Huang, Z. Luo, L. Liu, Y. Lu, Y. Li, L. Li, J. Hu, H. Ma, J. Chen, *Sci. Adv.* **2018**, *4*, eaao1761; b) W. Sun, F. Wang, B. Zhang, M. Zhang, V. Küpers, X. Ji, C. Theile, P. Bieker, K. Xu, C. Wang, *Science* **2021**, *371*, 46.
- [5] a) L. Cao, D. Li, E. Hu, J. Xu, T. Deng, L. Ma, Y. Wang, X.-Q. Yang, C. Wang, *J. Am. Chem. Soc.* **2020**, *142*, 21404; b) S. Wang, Z. Yuan, X. Zhang, S. Bi, Z. Zhou, J. Tian, Q. Zhang, Z. Niu, *Angew. Chem.* **2021**, *133*, 7132.
- [6] H. Qiu, X. Du, J. Zhao, Y. Wang, J. Ju, Z. Chen, Z. Hu, D. Yan, X. Zhou, G. Cui, *Nat. Commun.* **2019**, *10*, 5374.
- [7] a) W. Du, E. H. Ang, Y. Yang, Y. Zhang, M. Ye, C. C. Li, *Energy Environ. Sci.* **2020**, *13*, 3330; b) Z. Liu, Y. Yang, S. Liang, B. Lu, J. Zhou, *Small Struct.* **2021**, *2*, 2100119; c) J. Zheng, Q. Zhao, T. Tang, J. Yin, C. D. Quilty, G. D. Renteros, X. Liu, Y. Deng, L. Wang, D. C. Bock, *Science* **2019**, *366*, 645.
- [8] a) J. Hao, J. Long, B. Li, X. Li, S. Zhang, F. Yang, X. Zeng, Z. Yang, W. K. Pang, Z. Guo, *Adv. Funct. Mater.* **2019**, *34*, 1903605; b) L. Yuan, J. Hao, C. Kao, C. Wu, H. Liu, S. X. Dou, S. Z. Qiao, *Energy Environ. Sci.* **2021**, *14*, 5669; c) L. Ma, M. A. Schroeder, O. Borodin,

- T. P. Pollard, M. S. Ding, C. Wang, K. Xu, *Nat. Energy* **2020**, *5*, 743; d) Q. Zhang, J. Luan, X. Huang, Q. Wang, D. Sun, Y. Tang, X. Ji, H. Wang, *Nat. Commun.* **2020**, *11*, 3961.
- [9] N. Zhang, S. Huang, Z. Yuan, J. Zhu, Z. Zhao, Z. Niu, *Angew. Chem., Int. Ed.* **2021**, *60*, 2861.
- [10] a) Z. Zhao, J. Zhao, Z. Hu, J. Li, J. Li, Y. Zhang, C. Wang, G. Cui, *Energy Environ. Sci.* **2019**, *12*, 1938; b) Q. Zhang, J. Luan, L. Fu, S. Wu, Y. Tang, X. Ji, H. Wang, *Angew. Chem., Int. Ed.* **2019**, *58*, 15841.
- [11] D. Han, C. Cui, K. Zhang, Z. Wang, J. Gao, Y. Guo, Z. Zhang, S. Wu, L. Yin, Z. Weng, *Nat. Sustainable* **2021**, *5*, 205.
- [12] a) L. Ma, Q. Li, Y. Ying, F. Ma, S. Chen, Y. Li, H. Huang, C. Zhi, *Adv. Mater.* **2021**, *33*, 2007406; b) X. Zeng, J. Mao, J. Hao, J. Liu, S. Liu, Z. Wang, Y. Wang, S. Zhang, T. Zheng, J. Liu, *Adv. Mater.* **2021**, *33*, 2007416.
- [13] a) X. Wu, Y. Xu, C. Zhang, D. P. Leonard, A. Markir, J. Lu, X. Ji, *J. Am. Chem. Soc.* **2019**, *141*, 6338; b) N. Zhang, F. Cheng, Y. Liu, Q. Zhao, K. Lei, C. Chen, X. Liu, J. Chen, *J. Am. Chem. Soc.* **2016**, *138*, 12894.
- [14] a) L. L. Jiang, C. Yan, Y. X. Yao, W. Cai, J. Q. Huang, Q. Zhang, *Angew. Chem., Int. Ed.* **2021**, *60*, 3402; b) X. Ren, S. Chen, H. Lee, D. Mei, M. H. Engelhard, S. D. Burton, W. Zhao, J. Zheng, Q. Li, M. S. Ding, *Chem* **2018**, *4*, 1877.
- [15] a) A. Naveed, H. Yang, J. Yang, Y. Nuli, J. Wang, *Angew. Chem., Int. Ed.* **2019**, *58*, 2760; b) W. Kao-ian, M. T. Nguyen, T. Yonezawa, R. Pornprasertsuk, J. Qin, S. Siwamogsatham, S. Kheawhom, *Mater. Today Energy* **2021**, *21*, 100738.
- [16] a) Z. Liu, T. Cui, G. Pulletikurthi, A. Lahiri, T. Carstens, M. Olschewski, F. Endres, *Angew. Chem., Int. Ed.* **2016**, *55*, 2889; b) H. Yang, Z. Chang, Y. Qiao, H. Deng, X. Mu, P. He, H. Zhou, *Angew. Chem., Int. Ed.* **2020**, *59*, 9377.
- [17] T. Ohtsuka, M. Matsuda, *Corrosion* **2003**, *59*, 407.
- [18] S. Han, X. Hu, J. Wang, X. Fang, Y. Zhu, *Adv. Energy Mater.* **2018**, *8*, 1800955.
- [19] H. Yang, Y. Qiao, Z. Chang, H. Deng, P. He, H. Zhou, *Adv. Mater.* **2020**, *32*, 2004240.
- [20] a) S. Li, J. Fu, G. Miao, S. Wang, W. Zhao, Z. Wu, Y. Zhang, X. Yang, *Adv. Mater.* **2021**, *33*, 2008424; b) L. Ma, S. Chen, N. Li, Z. Liu, Z. Tang, J. A. Zapien, S. Chen, J. Fan, C. Zhi, *Adv. Mater.* **2020**, *32*, 1908121.
- [21] a) J. Hao, B. Li, X. Li, X. Zeng, S. Zhang, F. Yang, S. Liu, D. Li, C. Wu, Z. Guo, *Adv. Mater.* **2020**, *32*, 2003021; b) S. B. Wang, Q. Ran, R. Q. Yao, H. Shi, Z. Wen, M. Zhao, X. Y. Lang, Q. Jiang, *Nat. Commun.* **2020**, *11*, 1634.
- [22] J. Guo, J. Ming, Y. Lei, W. Zhang, C. Xia, Y. Cui, H. N. Alshareef, *ACS Energy Lett.* **2019**, *4*, 2776.
- [23] B. Akhsassi, A. Bouddouch, Y. Naciri, B. Bakiz, A. Taoufyq, C. Favotto, S. Villain, F. Guinneton, A. Benlhachemi, *Chem. Phys. Lett.* **2021**, *783*, 139046.
- [24] W. Zhang, Q. Zhao, Y. Hou, Z. Shen, L. Fan, S. Zhou, Y. Lu, L. A. Archer, *Sci. Adv.* **2021**, *7*, eabl3752.
- [25] J. Hao, X. Li, S. Zhang, F. Yang, X. Zeng, S. Zhang, G. Bo, C. Wang, Z. Guo, *Adv. Funct. Mater.* **2020**, *30*, 2001263.
- [26] C. Yan, H.-R. Li, X. Chen, X.-Q. Zhang, X.-B. Cheng, R. Xu, J.-Q. Huang, Q. Zhang, *J. Am. Chem. Soc.* **2019**, *141*, 9422.
- [27] N. Chang, T. Li, R. Li, S. Wang, Y. Yin, H. Zhang, X. Li, *Energy Environ. Sci.* **2020**, *13*, 3527.
- [28] a) Y. Jin, K. S. Han, Y. Shao, M. L. Sushko, J. Xiao, H. Pan, J. Liu, *Adv. Funct. Mater.* **2020**, *30*, 2003932; b) N. Zhang, F. Cheng, J. Liu, L. Wang, X. Long, X. Liu, F. Li, J. Chen, *Nat. Commun.* **2017**, *8*, 405.
- [29] S. J. Zhang, J. Hao, D. Luo, P. F. Zhang, B. Zhang, K. Davey, Z. Lin, S. Z. Qiao, *Adv. Energy Mater.* **2021**, *11*, 2102010.
- [30] Q. Yang, Q. Li, Z. Liu, D. Wang, Y. Guo, X. Li, Y. Tang, H. Li, B. Dong, C. Zhi, *Adv. Mater.* **2020**, *32*, 2001854.
- [31] E. Diler, B. Lescop, S. Rioual, G. N. Vien, D. Thierry, B. Rouvellou, *Corros. Sci.* **2014**, *79*, 83.
- [32] a) M. Zhao, B. Q. Li, H. J. Peng, H. Yuan, J. Y. Wei, J. Q. Huang, *Angew. Chem., Int. Ed.* **2020**, *59*, 12636; b) X. Xu, Y. Chen, D. Zheng, P. Ruan, Y. Cai, X. Dai, X. Niu, C. Pei, W. Shi, W. Liu, F. Wu, Z. Pan, H. Li, X. Cao, *Small* **2021**, *17*, 2101901; c) Q. Zhao, N. W. Utomo, A. L. Kocen, S. Jin, Y. Deng, V. X. Zhu, S. Moganty, G. W. Coates, L. A. Archer, *Angew. Chem.* **2022**, *134*, e202116214.
- [33] a) F. Wu, Y. Chen, Y. Chen, R. Yin, Y. Feng, D. Zheng, X. Xu, W. Shi, W. Liu, X. Cao, *Small* **2022**, *18*, 2202363; b) L. Li, L. Zhang, W. Guo, C. Chang, J. Wang, Z. Cong, X. Pu, *J. Mater. Chem. A* **2021**, *9*, 24325; c) D. Wang, D. Lv, H. Peng, N. Wang, H. Liu, J. Yang, Y. Qian, *Nano Lett.* **2022**, *22*, 1750.